Int. J. Heat Mass Transfer. Vol. 36, No. 6, pp. 1495–1504, 1993
Printed in Great Britain

0017-9310/93 $6.00 + 0.00

The effect of inlet flow distribution on catalytic conversion efficiency

EVANGELOS KARVOUNIS and DENNIS N. ASSANIS
Department of Mechanical and Industrial Engineering, University of Illinois at Urbana-Champaign, Urbana, IL 61801, U.S.A.

(*Received* 20 *March* 1992 *and in final form* 14 *July* 1992)

Abstract—A methodology is developed for analyzing the effect of non-uniform inlet flow distribution on the conversion efficiency of an automotive catalytic converter. The flow through the converter is treated as steady, incompressible, and isothermal. Conversion rates through the monolith passages are assumed to be diffusion-controlled. Under these assumptions, the equation governing one-dimensional laminarized flow with mass transfer through monolith passages simplifies to a form that can be solved analytically. A relation between concentration of reactants and passage length may thus be obtained, with flow velocity as a governing parameter. In order to determine the complex flow field through the diffuser, monolith, and nozzle sections of the converter, for various flow rates and passage diameters, a finite element code is used. The methodology is then utilized to predict the distribution of reactant concentrations across the monolith's outlet based on its inlet velocity distribution. The proposed approach is an effective design tool for optimizing the geometry and performance of an automotive catalytic converter.

1. INTRODUCTION

CATALYTIC converters have been widely used since the 1960s to reduce gaseous emissions from spark ignition engines. However, the enforcement of ultra low emission standards for the late 1990s necessitates dramatic improvements in the design and conversion efficiency of catalytic converters. A comprehensive modeling of the complex transport and chemical phenomena within catalytic converters is therefore required.

In the passages of a catalytic converter, exhaust gas molecules diffuse into the porous catalytic material where oxidizing reactions take place. Products of these reactions diffuse back to the flowing gas through the surface of the catalyst. The rate of this process depends on (i) mass transfer rates of exhaust molecules through concentration boundary layers on the gas side, and through catalytic porous media on the solid side and (ii) chemical reaction rates which are strong functions of temperature and reactant concentrations. As far as mass transfer rates are concerned, diffusion rates in concentration boundary layers depend on local velocity and temperature fields; diffusion rates in the solid side depend on concentration and temperature gradients, but are mainly governed by molecular sizes [1].

Chemical reaction rates are affected by temperature, which in turn is governed by the rate at which heat released by the reactions diffuses through the converter material. At low temperatures, chemical reaction rates are low and catalytic conversion performance is controlled by them. At high temperatures, mass transfer rates become the limiting factor in the conversion process [2]. The transition between these two rate-controlling modes is a very complicated phenomenon, usually referred to as 'lightoff', and has been the subject of intensive research [3, 4]. Hidden in the complex and highly-coupled chemical and mass transfer mechanisms is a parameter that not only affects the rates at which non-equilibrium processes occur, but also determines the time available for them, namely flow velocity.

In an ideal converter, the flow at the exit of the inlet diffuser would be uniform, and thus would be evenly distributed to all monolith passages. However, large diffuser cone angles, inlet pipe curvature effects, and partially developed inlet velocity profiles lead to non-uniform inlet velocity distributions [5]. Therefore the turbulent exhaust gas flow from the exhaust pipe into the diffuser separates from its walls and tends to enter the central channels of the converter [6]. Thus, the highest portion of exhaust gas flow passes through the center of the honeycomb with a velocity significantly higher than the ideal uniform one. As a result, the degree of pollutants' oxidation at the converter outlet is lower, and the overall conversion efficiency is reduced. In addition, the rate of poison deposition is higher at regions with higher mass flow rate [7]. Hence, besides non-uniform catalyst exploitation, flow non-uniformity at the converter inlet results in non-uniform poisoning.

The flow distribution across the honeycomb frontal area depends on the geometry of a specific design as well as on upstream and downstream boundary conditions. While previous studies have successfully predicted three-dimensional turbulent flow patterns inside various converter geometries [8], little emphasis has been placed on correlating flow field with conversion efficiency. Although such a correlation was introduced in ref. [9], it was based on flow predictions

NOMENCLATURE

A_i	constant of Arrhenius expression for reaction rate
C_1, C_2, C_3	constants in k–ε model
c	inertial coefficient
D_h	monolith channel hydraulic diameter
D_i	diffusivity for species i
E_{ai}	activation energy for oxidizing reaction of i pollutant
f	pressure drop coefficient
k	turbulent kinetic energy
k_i	reaction rate constant for i pollutant
L	monolith length
$\dot{m}_e$	exhaust gas mass flow rate
P	pressure
R	exhaust pipe radius
R_c	monolith block radius
Re_h	Reynolds number based on channel hydraulic diameter
$\langle rce \rangle$	relative conversion efficiency
S_i	overall conversion rate constant for i pollutant
T_{Re}	exhaust gas temperature for particular Reynolds number
t	time
U	time averaged flow velocity vector
u	in channel flow velocity
u^*	friction velocity
V	volume
x	generalized coordinate.

Greek symbols

ε	turbulence dissipation rate
η_{conv}	conversion efficiency
κ	permeability
μ	dynamic viscosity
μ_{eff}	porous effective viscosity
μ_{tot}	total flow (laminar and turbulent) viscosity
ν_t	turbulent eddy diffusivity
ρ	density
$\sigma_k, \sigma_\varepsilon$	turbulence model constants
τ	shear tensor
ϕ	porosity (void fraction)
ω	mass fraction.

Subscript

f	fluid
i	refers to gas species as well as flow direction
id	ideal
o	initial (monolith entry)
out	final (monolith exit)
p	porous.

Superscript

+	non dimensionalized to initial values.

which are not in reasonable agreement with actual flow patterns through the converter monolith. Therefore, the objective of this work is to develop a methodology for characterizing the effect of a non-uniform flow distribution at the converter inlet on the resulting catalytic conversion efficiency.

This paper is arranged as follows. First, the modeling assumptions and mathematical formulation governing flow and mass transfer through the various sections of the converter are presented. Then, it is shown how the finite element code FIDAP can be successfully utilized to determine the complex flow distribution through the catalytic converter. Along with the numerical flow solution, an analytical mass transfer model is developed to correlate velocity distribution at the monolith inlet with the resulting catalytic conversion efficiency. Thus, the effect of operating and design parameters on conversion efficiency can be characterized following solution of the flow equations. To illustrate the potential of the methodology, the conversion behavior of a simple test geometry is examined for various flow rates and passage diameters.

2. MODELING ASSUMPTIONS

To obtain the velocity distribution at the monolith entrance, equations governing flow inside the converter were solved using the computational fluid mechanics package FIDAP [10]. As shown in Fig. 1, three sections constitute the physical domain: (1) a short initial length of exhaust pipe and the diffuser, (2) the monolith and (3) the nozzle together with a short length of tail pipe. For the purpose of this study, a simple axisymmetric geometry was considered. Thus only half of the physical domain needed to be modeled.

The flow through the converter was modeled as steady, i.e. no flow pulsations were considered. For the operating conditions under which the converter is expected to deliver maximum performance, i.e. high engine load and speed, flow fluctuations are small compared to the mean gas velocity. Furthermore, the Mach number in all flow regions is not expected to exceed 0.1. Therefore, treating the exhaust gas as incompressible is a reasonable approximation [6].

Engine exhaust flows are highly turbulent. The additional momentum diffusion 'path' introduced by turbulence greatly affects flow distribution. Therefore turbulent flow calculations have been performed upstream and downstream of the monolith. However, the turbulent flow leaving the diffuser laminarizes in the monolith passages due to their very small hydraulic diameter (in-passage Reynolds numbers are unlikely to exceed 500). Proper discretization of the computational domain in order to solve for the flow in

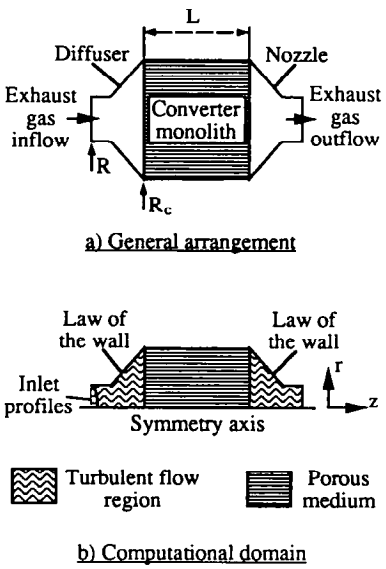

FIG. 1. Schematic of general arrangement.

all the monolith passages would render the calculation impractical. Instead, flow through the monolith has been solved utilizing FIDAP's ability to solve for flow through porous media. By properly adjusting the parameters of the governing Forchheimer–Brinkman equation, we could (i) force the flow to follow the direction of the passages, and (ii) reproduce the linear relation between flow velocity and pressure gradient which characterizes laminar flows in ducts.

The flow was treated as isothermal. Since it has already been assumed to be incompressible, the momentum and energy conservation equations are decoupled. As a result, flow field predictions would not be significantly affected by the isothermal approximation. Besides, under high load, high speed conditions, temperatures throughout the converter are high enough for conversion rates to be diffusion controlled, i.e. mainly a function of concentration of the local reactants [8].

Under the above assumptions, the equation governing one-dimensional flow with mass transfer through the converter channels simplifies to a form that can be solved analytically. A relation between concentration of reactants and passage length may thus be obtained, with flow velocity as a governing parameter. Therefore, given a velocity distribution at the monolith inlet and the monolith length, we could predict the distribution of reactant concentrations across its outlet. Following this methodology, the effect of flow distribution on catalytic conversion efficiency can be quantified.

3. MATHEMATICAL PROBLEM FORMULATION

3.1. *Flow modeling*

3.1.1. *Flow through the diffuser and nozzle sections.* For the diffuser and nozzle sections, equations governing steady, incompressible, turbulent flow [11] were solved. The time-averaged equation for mass conservation can be expressed as

$$\nabla \cdot \mathbf{U} = 0 \tag{1}$$

where $\mathbf{U}$ is the local (time-averaged) velocity vector. Similarly, the time-averaged equation for momentum conservation is

$$\rho \mathbf{U} \cdot \nabla \mathbf{U} = -\nabla P + \nabla \cdot \tau \tag{2}$$

where ρ and P are the local (time-averaged) fluid density and pressure, and τ is the shear stress tensor including viscous and turbulent contributions, i.e.

$$\tau = \mu_{\text{tot}} \nabla \mathbf{U} \tag{3}$$

with

$$\mu_{\text{tot}} = \mu + \rho \nu_t \tag{4}$$

where μ is laminar viscosity and ν_t is turbulent eddy viscosity. By expressing shear stress components as functions of the time-averaged flow field gradients, the effect of turbulence is accounted for by introducing additional momentum diffusion paths through increased viscosity. The standard k–ε approach has been used to correlate turbulent viscosity with time-averaged flow field gradients:

$$\nu_t = C_\mu \frac{k^2}{\varepsilon} \tag{5}$$

where k is turbulent kinetic energy, and ε is turbulent dissipation rate [12].

The evolution of turbulent kinetic energy and its rate of dissipation are governed by

$$\nabla \cdot (\mathbf{U} \cdot k) = \nabla \cdot \left(\frac{\nu_t}{\sigma_k} \nabla k \right) + G_k - \varepsilon \tag{6}$$

$$\nabla \cdot (\mathbf{U} \cdot \varepsilon) = \nabla \cdot \left(\frac{\nu_t}{\sigma_\varepsilon} \nabla \varepsilon \right) + \frac{\varepsilon}{k} (C_1 G_k - C_2 \varepsilon) \tag{7}$$

where G_k is the generation term for k, i.e.

$$G_k = \tau : \nabla \mathbf{U}. \tag{8}$$

Commonly-reported values for the dimensionless k–ε model constants have been adopted:

$$C_\mu = 0.09, \quad C_1 = 1.44, \quad C_2 = 1.92,$$

$$\sigma_k = 1.\ , \quad \sigma_\varepsilon = 1.3.$$

The boundary conditions applied to the domain of turbulent flow are summarized below:

Inlet. The velocity profile was prescribed at the inlet cross section according to a '1/7' law [13]. Further, the distribution of non-dimensionalized turbulent kinetic energy $k/(u^*)^2$ and non-dimensionalized turbulence dissipation rate $\varepsilon R/(u^*)^3$ were prescribed at the diffuser inlet for fully developed flow in a circular pipe [11]. Simple polynomials were fitted to the prescribed variables in order to facilitate their implementation in the FIDAP input file.

Outlet. At the outlet, zero stress boundary conditions were assumed. In reality, the flow may not be fully developed in the short tail pipe length modeled. However, since an accurate determination of the velocity pattern at the exit was beyond our scope, no special boundary treatment has been attempted.

Solid walls. The classical turbulent 'law of the wall' treatment has been applied to solid boundaries [14]. This feature is a standard option in the FIDAP code.

3.1.2. *Flow through the converter monolith.* This section describes how flow through the converter monolith passages can be effectively solved utilizing FIDAP's model for flow through porous media [10]. According to the Forchheimer–Brinkman model for porous flow, the governing equation can be written in Cartesian coordinates as:

$$\left(\frac{\rho c}{\sqrt{\kappa_i}}\|\mathbf{U}\|^m + \frac{\mu}{\kappa_i}U_i\right) = -\frac{\partial P}{\partial x_i} + \frac{\partial}{\partial x_i}\left[\mu_{\text{eff}}\left(\frac{\partial U_i}{\partial x_j} + \frac{\partial U_j}{\partial x_i}\right)\right] \quad (9)$$

where c is an inertial coefficient, $\|\mathbf{U}\|$ the magnitude of local velocity vector, μ_{eff} an effective viscosity and κ_i the permeability in the ith direction. Note that fluid velocities in equation (9) are volume-averaged, i.e.

$$U_i = \frac{1}{V}\int (U_i)_{\text{local}}\,\mathrm{d}V \quad (10)$$

which are related to pore-averaged velocities

$$(U_i)_p = \frac{1}{V_f}\int (U_i)_{\text{local}}\,\mathrm{d}V_f \quad (11)$$

through

$$U_i = \phi\cdot(U_i)_p \quad (12)$$

where $\phi = V_f/V$ is the porosity, most commonly referred to as 'void fraction', V the volume of the monolith over which averaging is performed, and V_f the portion of the monolith volume which is occupied by the fluid.

Equation (9) represents a generalization of the standard Darcy equations for non-isothermal flow in a saturated porous medium [15]. If $c = 0$, a Brinkman model is obtained. If $\mu_{\text{eff}} = c = 0$, the standard Darcy formulation is approached. To model flow through the monolith channels using equation (9), the following adjustments are made. The parameter c is set equal to 0 and the effective viscosity μ_{eff} is set to a very small value (compared to the fluid dynamic viscosity μ). This strategy decouples flow velocities at nodes along a given monolith radius, as desired, since passage walls actually separate adjacent exhaust gas streams.

The porosity κ_z in the axial direction is adjusted so that the reduced equation (9) reproduce the linear relation between pressure drop and flow velocity as for laminar flow in a duct of square cross section [16]. If D_h is the hydraulic diameter of the channel under consideration and $(U_z)_p$ is the porous-averaged flow velocity through the channel, the local Reynolds number is

$$Re_h = \frac{(U_z)_p D_h}{\nu} = \frac{U_z D_h}{\phi\nu} \quad (13)$$

and the friction factor is given by [16]

$$f = \frac{56.81}{Re_h} \quad (14)$$

with an associated pressure drop

$$-\frac{\mathrm{d}P}{\mathrm{d}z} = \frac{f}{D_h}\cdot\tfrac{1}{2}\rho(U_z)_p^2 = \frac{28.4\mu}{\phi D_h^2}U_z. \quad (15)$$

Setting κ_z equal to

$$\kappa_z = \frac{\phi D_h^2}{28.4} \quad (16)$$

we can readily verify that equation (9) for the z-direction reduces to equation (15), as desired for laminar flows. Further, the porosity κ_r in the radial direction is set to a very low value (usually three orders of magnitude lower than κ_z suffices) to effectively block the flow in the radial direction.

3.2. *Mass transfer modeling*

Mass transfer in the monolith passages can be modeled using the steady, one-dimensional species-conservation equation for laminar flow of a multi component fluid [17], i.e.

$$\frac{\mathrm{d}(\rho_i u)}{\mathrm{d}z} = \frac{\mathrm{d}}{\mathrm{d}z}\left[\rho D_i\frac{\mathrm{d}}{\mathrm{d}z}\left(\frac{\rho_i}{\rho}\right)\right] + \frac{\mathrm{d}\rho_i}{\mathrm{d}t} \quad (17)$$

where ρ_i is density of substance i (mass per unit of fluid volume), D_i is diffusivity of substance i into the fluid, and u is porous-averaged flow velocity. For our analysis, $u = (U_z)_p$ is a function of radial position (i.e. it does not change along z), and is determined from equation (15). Since the flow is considered to be incompressible, ρ is constant. Thus, equation (17) reduces to

$$D_i\frac{\mathrm{d}^2\rho_i}{\mathrm{d}z^2} - u\frac{\mathrm{d}\rho_i}{\mathrm{d}z} = -\frac{\mathrm{d}\rho_i}{\mathrm{d}t}. \quad (18)$$

The key assumption utilized below is that the rate of destruction of substance i is proportional to its local density, i.e.

$$\frac{\mathrm{d}\rho_i}{\mathrm{d}t} = -S_i\rho_i \quad (19)$$

with S_i a proportionality constant. A simple way to estimate S_i is described at the end of this section.

Using equation (19), the governing equation (18) reduces to

$$D_i\frac{\mathrm{d}^2\rho_i}{\mathrm{d}z^2} - u\frac{\mathrm{d}\rho_i}{\mathrm{d}z} = S_i\rho_i. \quad (20)$$

Equation (20) can be further simplified based on scaling considerations. Non-dimensionalizing density and axial position,

$$\rho_i^+ = \frac{\rho_i}{\rho_{0i}} \quad z^+ = \frac{z}{L}$$

where ρ_{0i} is density of substance i at converter entrance and L is converter length, we get

$$\frac{D_i}{L^2}\left(\frac{d^2\rho_i^+}{dz^{+2}}\right) - \frac{u}{L}\left(\frac{d\rho_i^+}{dz^+}\right) = S_i(\rho_i^+). \quad (21)$$

Terms in parentheses are now of the order of unity and their coefficients have units of inverse time. The following characteristic time scales can be readily identified: $t_D = L^2/D_i$ for diffusion process, $t_u = L/u$ for residence time in the channel, and $t_s = 1/S_i$ for catalytic reaction process. Using $D_i = 2.74 \times 10^{-5}$ m^2 s^{-1}, which corresponds to diffusion of CO_2 into air at 550°C [18], $L = 0.15$ m (a typical monolith length), and $u = 10$ m s^{-1} (a typical flowing velocity), we can demonstrate that $t_D = 820$ s is very large compared to $t_u = 0.015$ s. Thus, the diffusion term in equation (21) can be neglected. Obviously, t_s must be comparable to t_u, otherwise the catalyst would not be of any use! Based on the above considerations, equation (21) simplifies to

$$-u\frac{d\rho_i}{dz} = S_i\rho_i \quad (22)$$

with solution

$$\rho_i(z, r) = \rho_{0i}\exp\left(-\frac{S_i z}{u(r)}\right) \quad (23)$$

where the dependence on radial position is included. If we define $\omega_i = \rho_i/\rho$ as the mass fraction of substance i, the resulting global mass fraction at the outlet of the monolith will be:

$$\omega_{i,\text{out}} = \frac{1}{\dot{m}_c}\int_0^{R_c} \rho_{0i}\exp\left(-\frac{S_i L}{u(r)}\right)\phi u(r) 2\pi\, dr \quad (24)$$

where

$$\dot{m}_c = \rho U_{av}\pi R^2 \quad (25)$$

is exhaust gas mass flow rate, R_c the converter radius, and R the exhaust pipe radius. Equation (25) can then be rewritten as

$$\omega_{i,\text{out}} = \omega_{0i}\frac{2\phi}{U_{av}R^2}\int_0^{R_c}\exp\left(-\frac{S_i L}{u(r)}\right)u(r) r\, dr. \quad (26)$$

A catalytic conversion efficiency can then be computed from

$$\eta_{\text{conv}} = 1 - \frac{\omega_{i,\text{out}}}{\omega_{0i}}. \quad (27)$$

To isolate the effect of inlet velocity non-uniformity from the influence of other factors determining the reaction rate S_i, consider the ideal case of an exhaust gas which enters the monolith with a uniform velocity

$$u_{\text{id}} = \frac{U_{av}}{\phi}\left(\frac{R}{R_c}\right)^2. \quad (28)$$

This uniform inlet velocity distribution produces an exhaust concentration

$$(\omega_{i,\text{out}})_{\text{id}} = \omega_{0i}\exp\left(-\frac{S_i L}{u_{\text{id}}}\right) \quad (29)$$

with a corresponding ideal conversion efficiency

$$(\eta_{\text{conv}})_{\text{id}} = 1 - \frac{(\omega_{i,\text{out}})_{\text{id}}}{\omega_{0i}}. \quad (30)$$

A 'relative conversion efficiency' can thus be defined to characterize the effect of different velocity distributions, i.e.

$$\langle rce\rangle = \frac{\eta_{\text{conv}}}{(\eta_{\text{conv}})_{\text{id}}} = \frac{1 - \dfrac{\omega_{i,\text{out}}}{\omega_{0i}}}{1 - \dfrac{(\omega_{i,\text{out}})_{\text{id}}}{\omega_{0i}}}. \quad (31)$$

Equations (26), (29), (31) form the basis for post processing the results of the flow model.

Equation (29) can also be used to provide an estimate for the value of S_i. Assuming that at the design point the converter can convert substance i with an efficiency of 95%, then

$$\frac{(\omega_{i,\text{out}})_{\text{id}}}{\omega_{0i}} = \exp\left(-\frac{S_i L}{u_{\text{id}}}\right) = 0.05. \quad (32)$$

Therefore, the reaction rate constant for substance i can be modeled by

$$S_i = -\frac{\ln(0.05)u_{\text{id}}}{L} = -\frac{\ln(0.05)\,U_{av}R^2}{\phi L R_c^2}. \quad (33)$$

4. APPLICATION OF THE MODEL

4.1. *Basic arrangement*

An axisymmetric arrangement has been selected for the application of the present methodology. The principal dimensions of the test geometry are summarized in Table 1.

Table 1. Principal dimensions of test geometry

Exhaust pipe radius, R	0.026 m
Tail pipe radius	0.026 m
Monolith radius, R_c	0.100 m
Diffuser section length	0.095 m
Monolith length, L	0.150 m
Nozzle section length	0.150 m
Hydraulic diameter of converter passage, D_h	1.49 mm
Void fraction ϕ	0.695

4.2. *Range of operating conditions*

The range of operating conditions for which simulation studies are performed is presented in Table 2. The tabulated conditions are selected to correspond to realistic exhaust flow conditions under different combinations of engine speed and load. For each Reynolds number, the properties of the flowing medium have been assumed to be those of air at the given temperature.

4.3. *Results and discussion*

4.3.1. *Flow solution.* Flow streamlines for the baseline case ($Re = 30\,000$ and $D_h = 1.49$ mm) are plotted in Fig. 2(a). Clearly, treating the flow through the converter monolith using the flow through porous media feature of FIDAP produces the expected laminarized flow behavior within the converter channels. Also, this treatment is compatible with turbulent flow modeling for the sections upstream and downstream of the monolith. In the diffuser section, the separated flow stream emerging from the exhaust pipe impinges on the front face of the monolith. The subsequent redistribution of the flow in the converter channels is clearly illustrated. After following the direction of the monolith passages, streamlines converge in the nozzle section which accelerates the flow and leads it into the tail pipe.

The pressure contour plot, shown in Fig. 2(b), also provides some valuable information. Pressure gradients are steeper along the monolith centerline than at the peripheral section due to the higher flow velocity along the centerline. In Fig. 3 where the pressure distribution along the converter centerline is presented, three different flow regimes are distinguishable. In the diffuser section, pressure rises as the flow impinges on the converter's face where it is abruptly decelerated. The linear pressure drop across the monolith corresponds to laminar flow in the channels. Finally, at the nozzle exit section, pressure is converted to kinetic energy as the flow enters the tailpipe.

Nevertheless, pressure gradients across the monolith, and especially at its exit, are very small (see Fig. 2(b)). It is therefore anticipated that by neglecting the final nozzle section and applying zero stress boundary conditions at the converter outlet we might obtain the same velocity distribution at the converter inlet. Such a modeling strategy would result in significant savings in computation time.

To test this postulate, flow computations have been carried out for the complete converter geometry versus the diffuser and monolith sections only. As shown, in Fig. 4, the computed radial distribution of the axial velocity at the converter inlet is virtually the same for both simulations. Hence, disregarding computation of the flow through the nozzle section is acceptable for the purpose of predicting the velocity distribution at the monolith inlet. However, if the overall converter pressure drop is to be determined, flow development throughout the complete configuration must be modeled.

Table 2. Range of operating conditions

Reynolds number	Exhaust gas temperature (°C)
8800	350
15 000	450
30 000	550
45 000	650
62 000	750

4.3.2. *Catalytic conversion efficiency.* Having optimized the overall solution procedure, two series of parametric runs are performed. First, the exhaust pipe Reynolds number is varied while keeping the size of the monolith channels constant. Thus, conversion efficiency of the monolith can be examined at different flow rates. Then, the hydraulic diameter of the channels is varied at constant Re number. Hence, the influence of monolith flow resistance on conversion efficiency, as well as on other design trade-offs, can be revealed.

Radial distributions of the computed axial velocity across the inlet of the monolith are plotted in Fig. 5 for different Reynolds numbers. Since the flow velocities correspond to different flow rates, they have been normalized with respect to their maximum value in order to be comparable. It is clearly shown that flow non-uniformity increases with increasing flow rate. And this confirms that, at high engine loads and speeds, i.e. when the catalytic converter is expected to perform at its best, it actually suffers the highest efficiency loss due to the flow maldistribution problem.

In order to quantify the effect of inlet flow non-uniformities on conversion efficiency, care is needed in choosing the reaction rate parameter to be used in our analytical model. One approach would be to select, at each flow rate, the reaction rate parameter S_i which would produce a specified ideal conversion efficiency for a uniform inlet velocity distribution (Case A). The relative conversion efficiency which was computed in this fashion is presented along with the ideal one in Fig. 6(a). Since the parameter S_i is recalculated for each Reynolds number, the ideal conversion efficiency is constant (in this case 95%). The relative conversion efficiency, $\langle rce \rangle$, is close to unity at very low Reynolds numbers, and then starts dropping until reaching $\langle rce \rangle = 0.84$ at $Re = 62\,000$.

It can be argued, however, that it is more reasonable to assume that the value of S_i, optimized only at the design point, remains constant over the entire operating envelope (Case B). To examine this assumption, the value of S_i is calculated assuming an ideal efficiency of 95% at $Re = 62\,000$. Then, with decreasing flow rates, the ideal efficiency would increase until perfect conversion is achieved at $Re = 45\,000$ (see Fig. 6(b)). In this case, at low Reynolds numbers, the actual conversion efficiency coincides with the ideal conversion efficiency. This suggests that the effect of

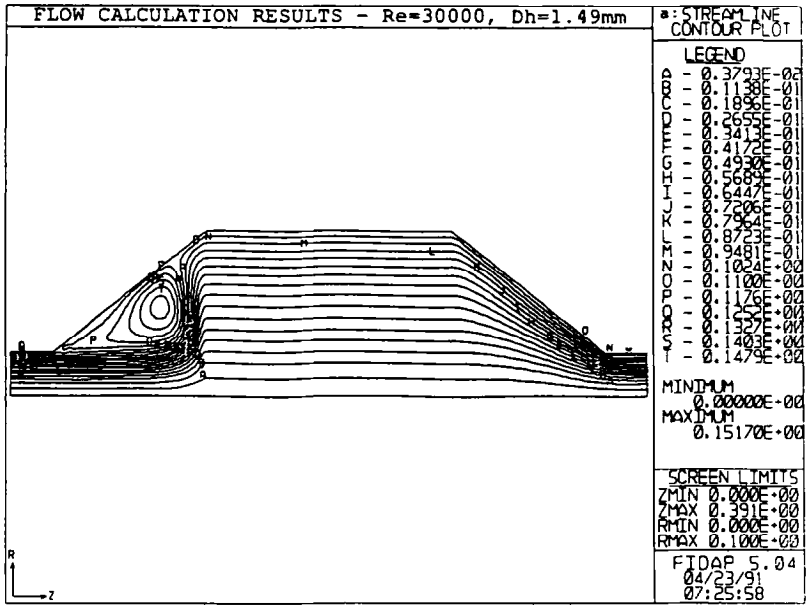

(a)

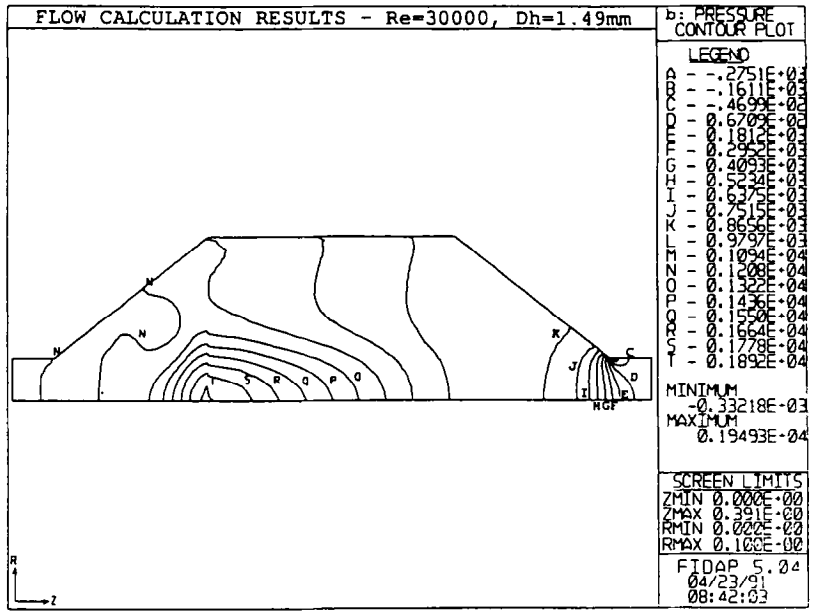

(b)

FIG. 2. Flow solution results at $Re = 30\,000$, $D_h = 1.49$ mm. (a) Flow streamlines. (b) Pressure contour plot.

inlet flow distortion is minimal at low flow rates. However, at high flow rates, the relative conversion efficiency behaves as for the case of constant ideal conversion efficiency.

A third possible approach is to take into consideration the effect of temperature changes on the reaction rate, as well. It can be found [9] that the reaction rate constant for the catalytic oxidation of both carbon monoxide and unburned hydrocarbons can be expressed as:

$$k_i = A_i \cdot \exp\left(-\frac{E_{ai}}{R \cdot T}\right)$$

where i refers to CO or HC, A_i is a constant, and the ratio of activation energy to gas constant E_{ai}/R is 8944 K for both species. Then, the reaction rate parameter S_i is calculated for $Re = 62\,000$, and subsequently corrected at lower flow rates according to the ratio

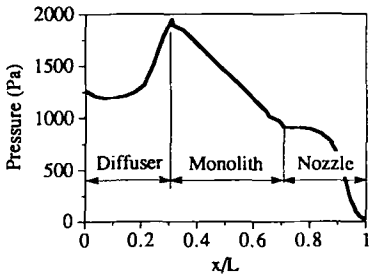

FIG. 3. Pressure distribution along centerline (Re = 30 000, D_h = 1.49 mm).

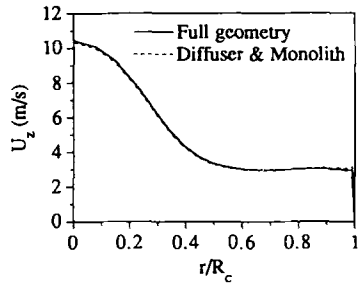

FIG. 4. Radial distribution of axial velocity at the inlet of converter monolith. Comparison between solutions obtained by modeling the complete converter geometry versus the diffuser and monolith sections only (Re = 30 000, D_h = 1.49 mm).

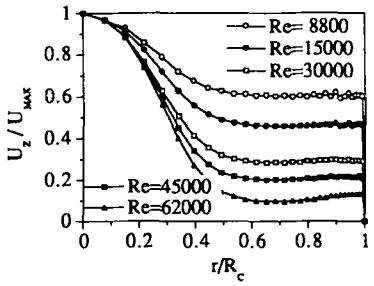

FIG. 5. Radial distribution of normalized axial velocity at the inlet of converter monolith for different exhaust pipe Reynolds numbers (D_h = 1.49 mm).

$$\frac{\exp\left(-\frac{8944}{T_{Re}[\mathrm{K}]}\right)}{\exp\left(-\frac{8944}{T_{62\,000}[\mathrm{K}]}\right)}.$$

Results calculated according to this scenario (Case C) are presented in Fig. 6(c). Contrary to the previous two cases, the ideal conversion efficiency dramatically drops with decreasing flow rates due to the lower reaction rates. Recall that low flow rates are accompanied by low exhaust gas temperatures. On the other hand, the effect of temperature correction on relative conversion efficiency is minimal, since the latter primarily reflects inlet flow distortion.

The combined effect of reaction rate and inlet flow distortion is captured by the product of ideal and relative conversion efficiencies. The resulting actual conversion efficiencies, calculated according to the previous three approaches, are plotted in Fig. 6(d). Correcting the reaction rate using the Arrhenius chemical kinetics formula (Case C) overestimates the actual decrease of the conversion efficiency at high Re. Above 350°C, the light-off point of the converter has already been exceeded, and the chemical reaction rate is no longer the main governing factor. However, conversion rates increase with increasing Re due to the associated higher diffusion rates. Thus, assuming a constant reaction rate parameter (as in Case B) is not realistic, either. Thus, the first approach, i.e. using different values of S_i for each Re number (Case A) seems to be closer to reality.

The next parameter to be investigated with the present model is monolith resistance. The hydraulic diameter of the converter channel is varied and its effect on conversion efficiency is quantified. Mass transfer rates through the converter channel surfaces are proportional to the ratio of channel perimeter over its cross-sectional area. Thus, catalytic conversion rates are expected to be inversely proportional to the channel hydraulic diameter. Therefore, S_i has been re-computed for each case with a converter length varying proportionally to D_h so that it gives an ideal conversion efficiency of 95% at the reference point of Re = 30 000, D_h = 1.49 mm. This effectively takes into account the reduction in conversion rate with increasing monolith length.

Radial distributions of the axial velocity at the monolith inlet are shown in Fig. 7 as a function of passage hydraulic diameter. It is evident that increasing monolith resistance improves the inlet velocity distribution, and thus relative conversion efficiency as shown in Fig. 8(a). On the other hand, the reduced passage diameter increases pressure drop for a given converter length, as illustrated in Fig. 8(b). However, the narrower channels allow for increased mass transfer rates. Consequently, the higher pressure drop associated with narrower channels can be partially recovered by reducing converter length (see Fig. 8(b)), thus taking advantage of its improved conversion efficiency.

5. CONCLUSIONS

In this work, a methodology has been developed for analyzing the effect of non-uniform inlet flow distribution on the conversion efficiency of an automotive catalytic converter. First, the finite element code FIDAP was successfully utilized to determine the flow distribution through the catalytic converter. Flow through sections upstream and downstream of the converter monolith was treated as steady, incompressible, and turbulent. The model for flow through

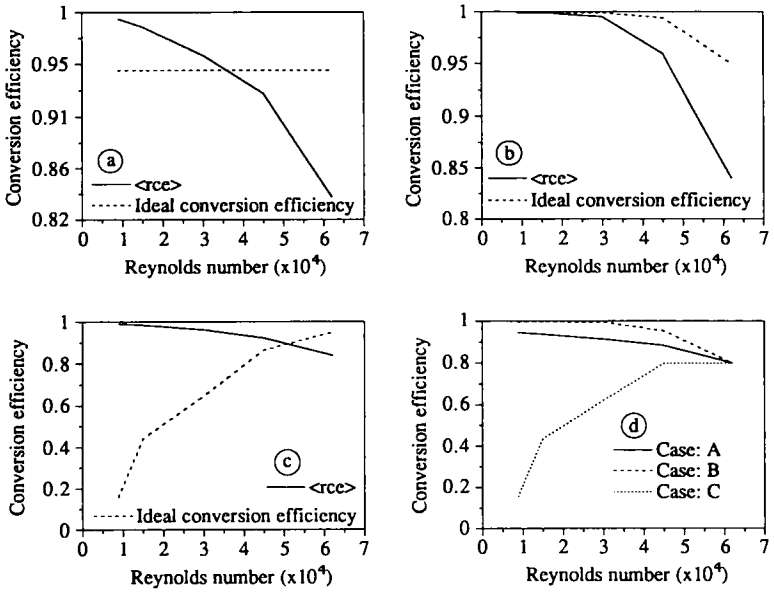

FIG. 6. Conversion efficiency versus Reynolds number. (a) Relative conversion efficiency conservatively optimized for each flow rate. (b) Relative conversion efficiency conservatively optimized at maximum flow rate. (c) Including effect of temperature on reaction rate. (d) Actual conversion efficiency (product of the ideal with the relative conversion efficiency).

porous media, incorporated in the FIDAP code, was suitably modified in order to reproduce the one-dimensional laminar flow behavior in the monolith channels. Along with the numerical flow solution, an analytical mass transfer model has been developed to correlate inlet velocity distribution and resulting catalytic conversion efficiency.

It has been found that the radial distribution of the axial velocity profile at the monolith inlet can be accurately predicted by modeling the flow through the diffuser and monolith sections of the converter, only. This strategy results in significant savings in computation time. However, if the pressure drop along the entire catalytic converter is to be determined, the flow through the nozzle downstream of the monolith has to be modeled.

The conversion behavior of a simple test geometry was examined while varying one operating parameter (Reynolds number) and one design parameter (passage diameter) at a time. It has been found that inlet velocity non-uniformity increases, and thus catalytic conversion efficiency decreases, as Reynolds number is increased. Unfortunately, high Reynolds numbers

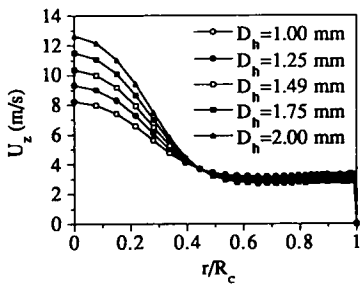

FIG. 7. Radial distribution of axial velocity at the inlet of converter monolith for different passage hydraulic diameters (Re = 30 000).

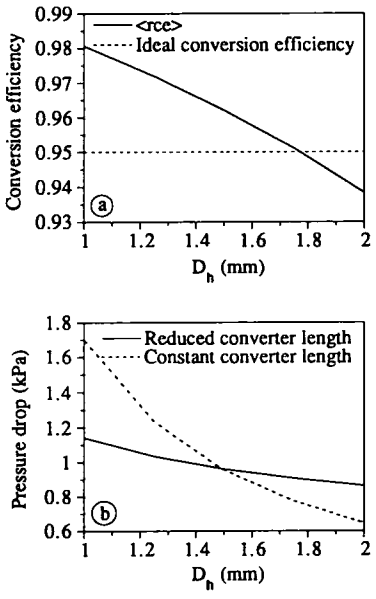

FIG. 8. Effect of passage hydraulic diameter. (a) On relative conversion efficiency. (b) On pressure drop along the monolith.

correspond to operating conditions where the highest performance is required from the device. Reducing the passage diameter, improves velocity distribution and, as a result, conversion efficiency, but also increases pressure drop. The latter side effect may be partially offset by making the converter shorter, thus taking advantage of its improved efficiency.

Acknowledgement—This material is based upon work supported by the National Science Foundation under Grant No. CBT-8858310. The authors gratefully acknowledge the National Center for Supercomputing Applications for providing computer time for the flow calculations on the CRAY Y-MP supercomputer.

REFERENCES

1. J. W. Fulton, Building the mathematical model of the catalyst and reactor, *Chem. Engng*, February 17, 118–124 (1986).
2. L. S. Socha, Jr., J. P. Day and E. H. Barnett, Impact of catalyst support design parameters on FTP emissions, *S.A.E.* Paper 892041 (1989).
3. S. H. Oh, J. C. Cavendish and L. L. Hegedus, Mathematical modeling of catalytic converter lightoff: single-pellet studies, *A.I.Ch.E. Jl* **26**(6), 935–943 (1980).
4. S. H. Oh and J. C. Cavendish, Mathematical modeling of catalytic lightoff Part II: Model verification by engine-dynamometer experiments, *A.I.Ch.E. Jl* **31**(6), 935–942 (1985).
5. J. S. Howitt and T. C. Sekella, Flow effects in monolithic honeycomb automotive catalytic converters, Paper 740244, *S.A.E. Trans.* **83**, 1067–1075 (1974).
6. D. W. Wendland and W. R. Matthes, Visualization of automotive catalytic converter internal flows, Paper 861554, *S.A.E. Trans.* **95**(6), 729–742 (1986).
7. M. C. Lai, J. Y. Kim, C. Y. Cheng, P. Li, G. Chui and J. D. Pakko, Three-dimensional simulations of automotive catalytic converter internal flow, *S.A.E.* Paper 910200 (1991).
8. D. K. S. Chen, S. H. Oh, E. J. Bissett and D. L. Van Ostrom, A three dimensional model for the analysis of transient thermal and conversion characteristics of monolithic catalytic converters, Paper 880282, *S.A.E. Trans.* **97**(3), 177–189 (1988).
9. G. Bella, V. Rocco and M. Maggiore, A study of inlet flow distortion effects on automotive catalytic converters, *Journal of Eng. for Gas Turbines and Power* **113**(3), 419–426 (1991).
10. Fluid Dynamics International, *FIDAP Theoretical Manual, Revision 6.0*. Evanston IL (1991).
11. J. O. Hinze, *Turbulence* (2nd Edn), p. 579. McGraw-Hill, New York (1959).
12. B. E. Launder and D. B. Spalding, *Mathematical Models of Turbulence*. Academic, New York (1972).
13. H. Schlichting, *Boundary Layer Theory* (7th Edn), p. 599. McGraw-Hill, New York (1979).
14. B. E. Launder and D. B. Spalding, The numerical computation of turbulent flow, *Comp. Meth. Appl. Mech. Eng.* **3**, (1974).
15. J. Bear, *Dynamics of Fluids in Porous Media*. American Elsevier, New York (1972).
16. F. M. White, *Fluid Mechanics* (2nd Edn), p. 331. McGraw-Hill, New York (1986).
17. D. B. Spalding, *Combustion and Mass Transfer* (1st Edn), p. 50. Pergamon Press, Oxford (1979).
18. F. P. Incropera and D. P. DeWitt, *Fundamentals of Heat and Mass Transfer*. Wiley, New York (1985).